Tribology Letters (2021) 69:147
https://doi.org/10.1007/s11249-021-01523-w

ORIGINAL PAPER

Prandtl–Tomlinson-Type Models for Molecular Sliding Friction

Sergio Javier Manzi[1] · Sebastian Eduardo Carrera[1] · Octavio Javier Furlong[1] · Germaine Djuidje Kenmoe[2,3] · Wilfred T. Tysoe[3]

Received: 11 August 2021 / Accepted: 26 September 2021 / Published online: 7 October 2021

Abstract

A model sliding potential, based on Prandtl–Tomlinson type models, is proposed for analyzing the temperature- and velocity-dependences of sliding processes at the interface between a tip and an adsorbed molecular layer. The proposed simple periodic potential has a parabolic form up to a critical distance, corresponding to the onset of detachment, at which point it becomes flat. The simplicity of the model will enable it to be used to analyze complex molecular interfaces, such as molecular films, mechanically induced chemical reactions or biological interfaces such as muscles or transport molecules. A simple analytical model is presented for the resulting velocity- and temperature-dependences of the friction force for the sliding of a compliant atomic force microscopy tip over an array of molecular species adsorbed on a surface, when only considering transitions of the tip in the forward direction (overall sliding direction). The validity of the analysis is tested by using kinetic Monte Carlo (kMC) simulations of the sliding over the molecular potential. This simulation provides excellent agreement with the analytic model, except for some slight differences that arise from the way in which the simulations calculate the lateral force compared to the analytical model. However, significant deviations are found between the kMC simulations and the analytical model when the possibility of both forward and reverse transitions are included, in particular at high sliding velocities and low temperatures. The origin of these effects are discussed in the manuscript, but result in superlubricious behavior, that is, vanishing friction, in particular at low sliding velocities.

Graphical Abstract

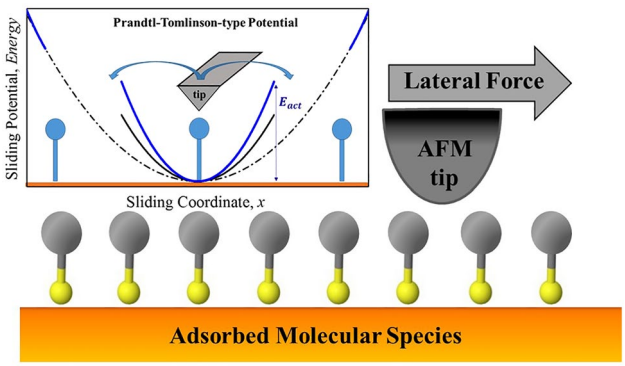

Keywords Prandtl–Tomlinson model · Friction · Organic surfaces · Monte Carlo simulations

1 Introduction

It has been recently demonstrated that the imposition of a force can induce mechano- or tribochemical reactions of molecules adsorbed on surfaces [1–8] with a rate that increases exponentially with applied stress in atomic force

✉ Wilfred T. Tysoe
wtt@uwm.edu

Extended author information available on the last page of the article

microscopy (AFM) experiments [9–12], in accord with the so-called Bell model [13]. However, little is known about how the force is exerted on the reacting molecular species at the sliding interface (the mechanophore), although it has been recently suggested that the nature of its terminal group, and the way it interacts with the moving counterface, can have a profound effect on the rate of a tribological reaction [14]. As a result, it would be useful to develop a model for sliding friction that can take into account the presence of adsorbed molecules on the sliding interface to enable tribochemical reactions to be included in the analysis.

The velocity and temperature dependences of the friction of solid surfaces measured in AFM [15–18] are commonly described by the Prandtl–Tomlinson (P–T) model [19, 20]. This model assumes that friction occurs as atoms in the contact slide over a periodic (generally sinusoidal) potential, where the energy is rapidly dissipated after surmounting the barrier. This approach has provided a fundamental understanding of the temperature- and velocity-dependences of sliding friction, as well as of the experimentally observed atomic stick–slip behavior [16, 21–25]. Here, the friction force is generally found to vary logarithmically with velocity up to a point at which the external force causes the energy barrier to decrease to zero, after which it becomes constant, as first predicted by Prandtl at the beginning of the last century [20].

The first nanoscale models of molecular friction were used to describe the contraction of skeletal muscles [26], where an analysis of the effect of a large number of interaction sites is known as the Lasker–Peskins model [27], while a model in which there are sparse interaction sites is known as the Huxley model [28]. These theories assume some kinetic model for the rates of attachment and detachment across the sliding interface [26]. Analogous models, which envisage the transient formation of bonds due to interactions across the sliding interface, have also been used to describe friction of solid–solid interfaces in general (rather than molecular sliding), such as proposed by Filippov et al. [29], where the rate of bond formation across the interface is assumed to be independent of distance. Here, the rate of bond scission is assumed to vary exponentially with the force acting on the bond multiplied by the bond extension for weak bonds, analogous to the Bell model [13], or an asymptotic form proposed by Prandtl for strong ones [20]. This general approach has recently been modified to include activated bond formation to explain unusual temperature dependences found in AFM friction measurements [30–32].

These approaches differ from the way in which the Prandtl–Tomlinson model is conventionally analyzed since, rather than describing the rates of bond formation and scission at the sliding interface as these models do, P–T theory models the dissipation of a compliant tip sliding over a corrugated potential due to the interaction between the tip and surface. The effect of the tip motion is to reduce the energy barrier for sliding, thereby increasing the rate at which the tip can surmount such barrier. The logarithmic dependence on sliding velocity arises naturally from this model [33, 34]. For example, in the case of a periodic potential with wavelength λ, to first order the energy barrier E_a is reduced by the imposition of a force F to $E_a - \frac{F\lambda}{2}$, analogous to the Bell model [13], where $\lambda/2$ is the distance from the initial state to the transition state. Thus, the rate constant for the transition over the barrier, k, is given by the transition-state theory as: $k = A\ \exp\left(\frac{E_a - F\lambda/2}{k_B T}\right)$, where T is the temperature, k_B is the Boltzmann constant and A is a pre-exponential factor. However, the rate of transition over the barrier is dictated by the sliding velocity v as $v = k\lambda$, so that the force automatically adjusts to lower the barrier in response to sliding. Equating k in both expressions leads to a simple formula for the velocity and temperature dependences of the friction force as:

$$F(v,T) = \frac{2E_a}{\lambda} + \frac{2k_B T}{\lambda}\ln\left(\frac{v}{\lambda A}\right) \tag{1}$$

Analogous behavior is found for many tribological phenomena [35], and these ideas underpin the analysis of sliding friction. Thus, the goal of the following paper is to propose and analyze a sliding potential that describes the interaction between an AFM tip and an array of molecules adsorbed equidistantly on a surface. In addition, since molecular adsorbates are themselves compliant, given that the portion of the molecule that is anchored to the surface can also distort under the influence of the applied force, the resulting potential should be such that it can easily couple to the rest of the molecule. This property can be expected to lead to unusual velocity dependences of the friction force; both $\ln(v)$ and more complex velocity dependences have been observed for adsorbed molecular layers [36–41], where in some cases, friction increases and then decrease as a function of velocity. Such unusual friction may arises due to the fact that the sliding molecular interface has multiple degrees of freedom that can be excited during sliding. For example, a simple molecular adsorbate can store energy by tilting with respect to the surface due to an interaction with the sliding tip. As another example, the friction of hydrogels shows a variable velocity-dependent [42–46], where such dependence is described by the competing effect of adhesive and viscous contributions [47]. Being able to include such additional degrees of freedom is also important for describing shear-induced tribo- or mechanochemical reaction rates of adsorbed molecular species.

In order to propose a suitable potential that will be useful for describing such phenomena, it is suggested that the interaction between a tip and the terminus of the molecular adsorbate will be similar in shape to a Morse [48] or Lennard–Jones potential. Indeed, the Morse potential has been

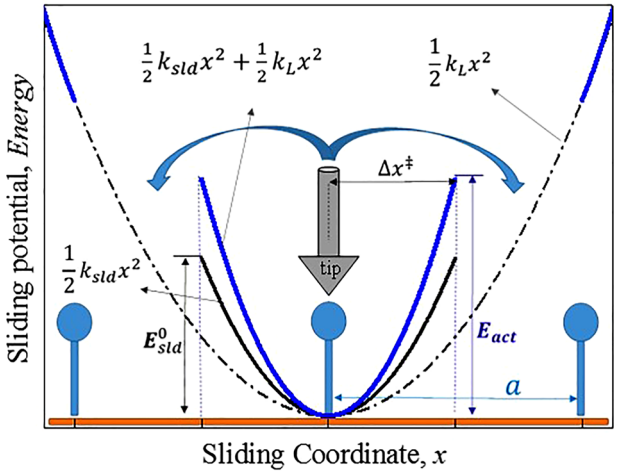

Fig. 1 Plot of the model's sliding potential, Eq. (4), used to describe the sliding of an AFM tip over an array of molecular adsorbates

used to describe the mechanically induced decomposition of polymers [33]. Such intermolecular potentials are also consistent with the shapes of force-distance curves measured by AFM [49], in which an initial attractive interaction can lead to a snap into contact, and the presence of a pull-off force indicates that the interaction between the tip and surface ceases. However, such a form of the potential will make it difficult to model the effect of coupled systems, such as simultaneous sliding and chemical reactions. Thus, the proposed form of the sliding surface potential is shown in Fig. 1, where a parabolic variation in energy is plotted versus the sliding coordinate, until a critical distance is reached at which the tip detaches and can move to attach to an adjacent site located at a distance a away. Thus, the periodicity of the adsorbates is taken to be equal to a. Similar forms of this potential have been used to model reaction energy profiles in Evans-Polanyi [50] models or Marcus theory [51]. It is assumed that the unperturbed adsorbate is defined at $x = 0$, and has a minimum energy at this value, so that the sliding surface potential can be expressed as $V_S(x) = \frac{1}{2}k_{sld}x^2$, where k_{sld} is the force constant, and is only valid while the tip is in contact with (attached to) the adsorbed species. It is also assumed that this interaction varies smoothly until reaching a sliding activation energy E^0_{sld} (Fig. 1, solid black line), that is, when the sliding coordinate reaches a value of $\Delta x^{\ddagger}$ (note that for the case of Fig. 1, $\Delta x^{\ddagger} = 0.5a$), therefore:

$$k_{sld} = \frac{2E^0_{sld}}{\left(\Delta x^{\ddagger}\right)^2} \tag{2}$$

In this case, the surface energy profile is given by:

$$V_S(x) = E^0_{sld}\left(\frac{x}{\Delta x^{\ddagger}}\right)^2 \tag{3}$$

In the following, the conventional P–T model is extended to sliding over a rigid molecularly adsorbed overlayer using the form of the potential described above such that the molecule itself does not tilt under the influence of the lateral force. This will set the stage for analyzing more complex interfaces with several, coupled degrees of freedom. Such an analysis will be given in future papers, and this manuscript focusses on analyzing the behavior of this simple model potential.

We first provide an analytical solution to the model using strategies analogous to those used for the conventional P–T model for a sinusoidal potential (see Supplementary Material section). Note that the parabolic form of the sliding potential described in Eq. (3) is easier to analyze than the classical P–T model for a sinusoidal periodic potential.

A common strategy used for analyzing the dynamics of the Prandtl–Tomlinson model, similar to the approach used by Eyring [33, 34], described briefly above, uses transition-state theory to describe the rate of transition over the energy barrier, where the pre-exponential factor is assumed to be insensitive to the external force [52, 53]. Here, it is implicitly assumed that the rate of energy dissipation after surmounting the energy barrier is extremely fast, thereby giving rise to the characteristic slick-slip behavior in the friction force [54]. In the present work, this model is analyzed using Monte Carlo (MC) methods [55–58] to include additional effects such as backward motions of the tip and to provide a test of the analytical model.

2 Analytical Prandtl–Tomlinson Model for Molecular Sliding

The Prandtl–Tomlinson model is analyzed for a surface potential $V_S(x)$, where the molecular adsorbates are assumed to be anchored to the surface at an evenly spaced distance a (see Fig. 1). From Eq. (3), where x represents the tip position, and, considering that the cantilever position is given by X (see Supplementary Materials section), both being along the sliding direction and coupled by an elastic force constant k_L, then the overall sliding potential is given by:

$$V_{tot}(x, X) = E^0_{sld}\left(\frac{x}{\Delta x^{\ddagger}}\right)^2 + \frac{1}{2}k_L(X - x)^2 \tag{4}$$

which is valid for $-\Delta x^{\ddagger} \le x \le \Delta x^{\ddagger}$. Following the analytical strategy outlined in the Supplemental Materials section, it is found that the energy minimum (V_{min}) occurs when:

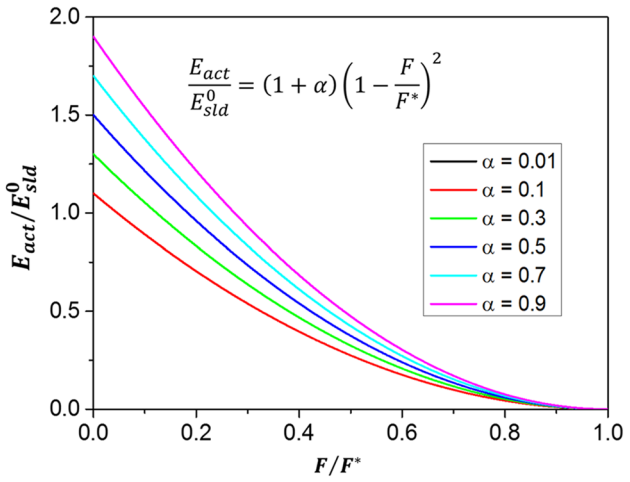

Fig. 2 Activation Energy (E_{act}/E^0_{sld}) vs. Lateral Force (F/F^*) for different values of $\alpha = \frac{k_L}{k_{sld}}$

$$\frac{\partial V_{tot}}{\partial x} = 0 = k_{sld}x - k_L(X-x) \tag{5}$$

so that

$$x_{min} = \frac{k_L}{k_{sld}+k_L}X \tag{6}$$

The energy maximum (V_{max}) occurs at $x = \Delta x^{\ddagger}$; therefore, the energy barrier $E_{act} = \Delta V = V_{max} - V_{min}$, can be obtained by replacing x by x_{max} and x_{min} into Eq. (4), to give:

$$E_{act} = V_{max} - V_{min} = E^0_{sld} + \frac{1}{2}k_L\left(X-\Delta x^{\ddagger}\right)^2 - \frac{1}{2}\frac{k_{sld}k_L}{k_{sld}+k_L}X^2 \tag{7}$$

In order to evaluate the behavior of the system with respect to the lateral force, it is convenient to express Eq. (7) in terms of F. Given that $F = k_L\left(X - x_{min}\right)$, from Eq. (3):

$$F = k_L\left(X - \frac{k_L}{k_{sld}+k_L}X\right) = \frac{k_Lk_{sld}}{k_{sld}+k_L}X \tag{8}$$

Substituting Eqs. (8) in (7) gives (for more details see Supplemental Material section):

$$E_{act}(F) = \frac{1}{2}\left(k_{sld}+k_L\right)\left(\Delta x^{\ddagger} - \frac{F}{k_{sld}}\right)^2 \tag{9}$$

Furthermore, considering Eq. (2) and introducing a parameter $\alpha = \frac{k_L}{k_{sld}}$, Eq. (9) can be written as:

$$E_{act}(F) = (1+\alpha)E^0_{sld}\left(1 - \frac{\alpha F}{k_L\Delta x^{\ddagger}}\right)^2 \tag{10}$$

so that the force at which the energy barrier vanishes is $F^* = \frac{k_L\Delta x^{\ddagger}}{\alpha} = k_{sld}\Delta x^{\ddagger}\frac{2E^0_{sld}}{\Delta x^{\ddagger}}$. Thus, $E_{act}(F) = (1+\alpha)E^0_{sld}\left(1-\frac{F}{F^*}\right)^2$ (see Fig. 2), which describes the change in activation energy with lateral force. Analogous to the Prandtl–Tomlinson model with a sinusoidal potential [16], the rate of transition over the energy barrier is given by (for more details, see Supplemental Material section):

$$\frac{dP(F)}{dF} = -\frac{A\left(k_{sld}+k_L\right)}{k_{sld}k_Lv}\exp\left(-\frac{E_{act}(F)}{k_BT}\right)P(F) \tag{11}$$

where A is a pre-exponential frequency factor. Since the maximum probability is given by $\frac{d^2P(F)}{dF^2} = 0$, we have:

$$\frac{1}{k_BT}\frac{dE_{act}(F)}{dF} + \frac{A\left(k_{sld}+k_L\right)}{k_{sld}k_Lv}\exp\left(-\frac{E_{act}}{k_BT}\right) = 0 \tag{12}$$

Furthermore, from Eq. (10):

$$\frac{dE_{act}(F)}{dF} = -\frac{2\left(k_{sld}+k_L\right)}{k_{sld}}\frac{E^0_{sld}}{F^*}\left(1-\frac{F}{F^*}\right) \tag{13}$$

Finally, substituting into Eq. (12) and rearranging gives:

$$\frac{1}{\beta k_BT}\left(1-\frac{F}{F^*}\right)^2 = \ln\left(\frac{v_0}{v}\right) - \ln\left(1-\frac{F}{F^*}\right) \tag{14}$$

where $\beta = \frac{2}{(k_{sld}+k_L)\Delta x^{\ddagger 2}}$, and $v_0 = \frac{Ak_BT}{k_L\Delta x^{\ddagger}}$, for the velocity and temperature dependences for an AFM tip sliding over a molecular adsorbate. The accuracy of this model is tested in the following section using kinetics Monte Carlo (kMC) simulations.

3 Kinetic Monte Carlo Simulations of the Prandtl–Tomlinson Model for Molecular Sliding

Kinetic Monte Carlo (kMC) simulations are used to solve the molecular P–T model, which, by including the possibility of both forward and reverse transitions, inherently includes the possibility of the tip reattaching, which is not included in the analytical model [55, 56]. The transition rate is calculated using the force-dependent activation barrier (Eq. (10)), where the transition rate w can be described by:

$$w(t) = A\exp\left[-\frac{E_{act}(t)}{k_BT}\right] \tag{15}$$

where A is the frequency attempt of a transition. For each MC trial, the value of w is calculated at some time t and compared to a random number ξ_1 uniformly distributed in the interval (0,1). If $\xi_1 < w$ the transition is allowed to occur, where both backward and forward transitions are allowed.

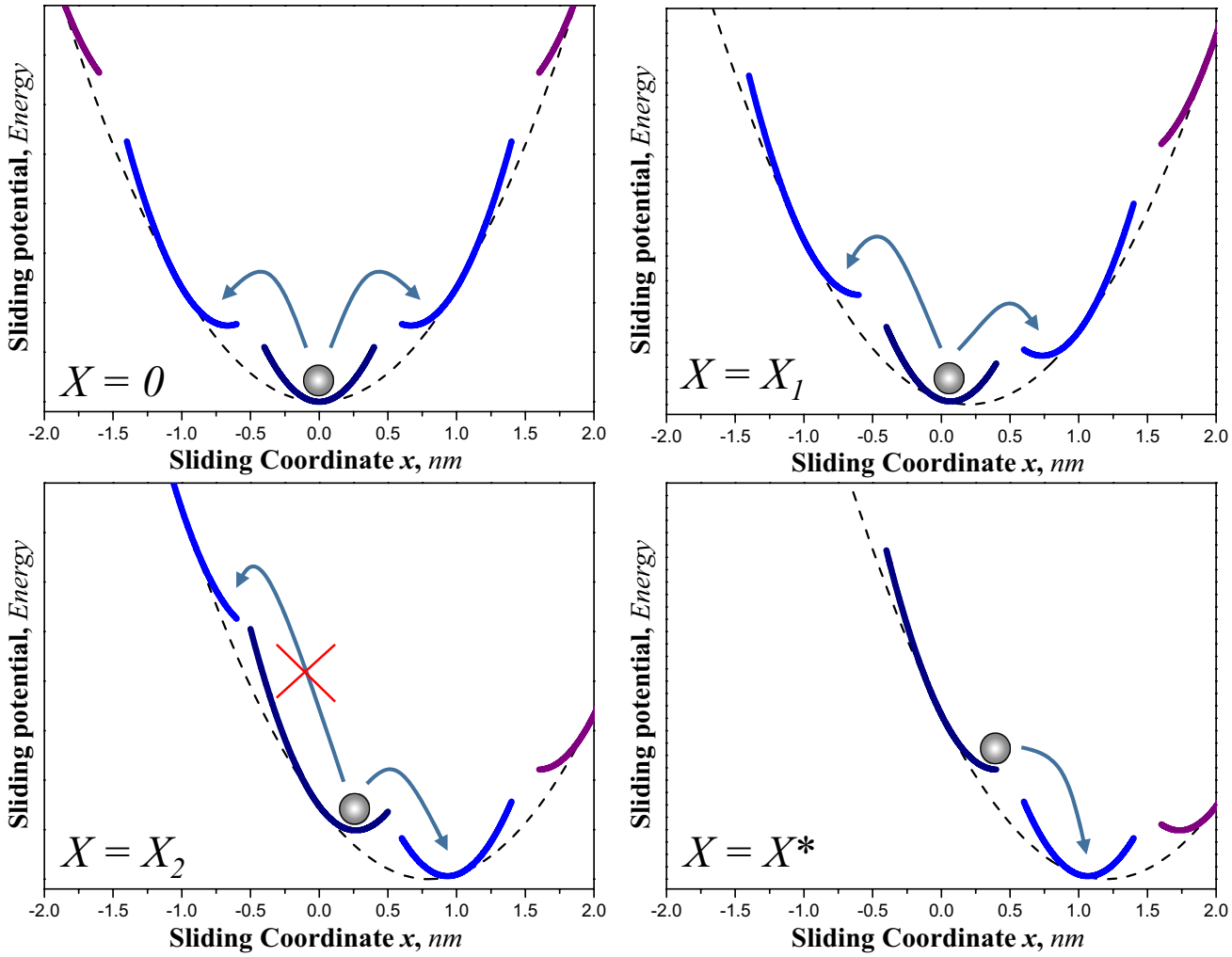

Fig. 3 Evolution of the energy barrier as a function of the support position X, for $X=0<X_1<X_2<X^*$, where X^* corresponds to the position value at which the energy barrier vanishes ($E_{act}=0$)

Finally, the lateral force is recorded as a function of time. The process is repeated a sufficient number of times to yield an average friction force with negligible statistical error. The conversion between MC time and real time is made by defining an elementary transition probability per unit time [59]. Such simulations provide the overall average lateral force at which the system overcomes the energy barrier and moves in the sliding direction.

Figure 3 illustrates the general evolution of the sliding potential as the tip is dragged over the adsorbed molecular layer. As can be observed, for the set of chosen parameters, when the support has not been displaced ($X=0$), there are local minima (stable positions) on both sides of the tip, so that it has the possibility of moving either forwards or backwards. As the support moves to the right ($0<X_1<X_2$), the probability of the tip moving forwards increases, while the probability of moving backwards decreases until there is eventually no stable position to the left, and the tip can only move forwards. Finally, if the support reaches its critical value (X^*), that is, when the energy barrier vanishes, the tip will immediately jump forward to the next stable position. Note that this last scenario is the only sliding mechanism allowed at $T=0\ K$.

In order to validate the kMC simulations, we first ran simulations only allowing forward transitions to occur to be able to directly compare with the analytical results described above (Eq. (14)). Typical van der Waals' radii are ~ 0.15 nm [60], so taking the intermolecular interaction between the tip and organic films to disappear at ~ 3 times the van der Waals' radius, gives $\Delta x^{\ddagger} \sim 0.45$ nm (for simplicity we set $a=1$ nm and $\Delta x^{\ddagger}=0.5a$). We use the form of the energy barrier in Eq. (3), which is assumed to be periodic, and if a is the periodicity of the interaction potential, $V_S(x) = V_S(x+a)$, we have:

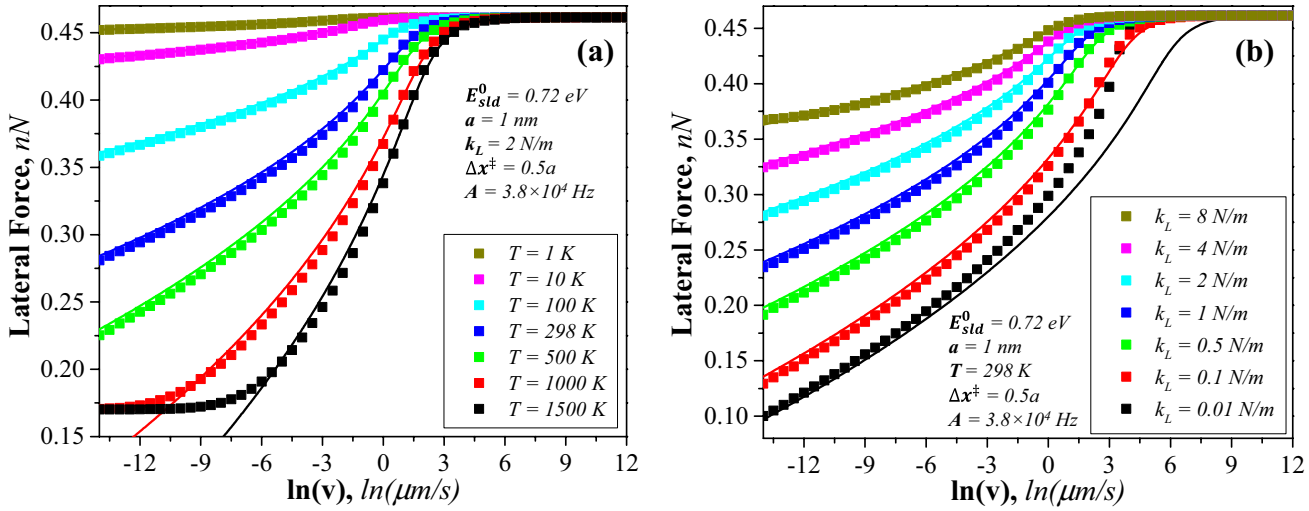

Fig. 4 Comparison between analytical (Eq. (14), solid lines) and MC results (symbols) where only forward transitions are allowed for **a)** lateral force versus ln(v) at different temperatures, and **b)** lateral versus ln(v) for different values of k_L

$$V_S(x) = \begin{cases} 1/2 k_{sld} x^2 \; if \; x < \Delta x^‡ \\ E^0_{sld} \; if \; x = \Delta x^‡ \\ 0 \; if \; \Delta x^‡ < x < a \end{cases} \tag{16}$$

To compare with the analytical model, we consider a system where $E^0_{sld} = 0.72$ eV, $a = 1$ nm, and $\Delta x^‡ = 0.5a$, for different values of T and k_L, using a pre-exponential factor of 3.8×10^4 s^{-1} (see below for a rationale for this choice of pre-exponetial factor). The results are shown in Fig. 4, where the solid lines represent the analytical solution (Eq. 14), and the solid squares are from the kMC simulations, where only forward transitions are allowed. As can be seen, the kMC simulations are in very good agreement with the analytical results.

However, some deviations are observed, which as describe below, begin to show the limitations of the analytical results. For example, a small deviation can be observed in Fig. 4a, where, for intermediate and low velocities, the simulated results are slightly lower than the analytical ones. This is attributed to the fact that the transition probability curve is asymmetric, so while the analytical results are based on calculating the maximum of the probability curve, the MC results calculate the average lateral force at which the system undergoes a transition, thus leading to these slight differences (see Supplementary Materials for more details). In addition, a more significant deviation can be observed in Fig. 4b as the value of k_L decreases, where the simulated results are higher than the analytical ones. This latter deviation is attributed to "memory effects", which are not considered in the analytical solutions (see Supplementary Materials for more details). While the analytical results provide the position at which the tip will detach (lateral force),

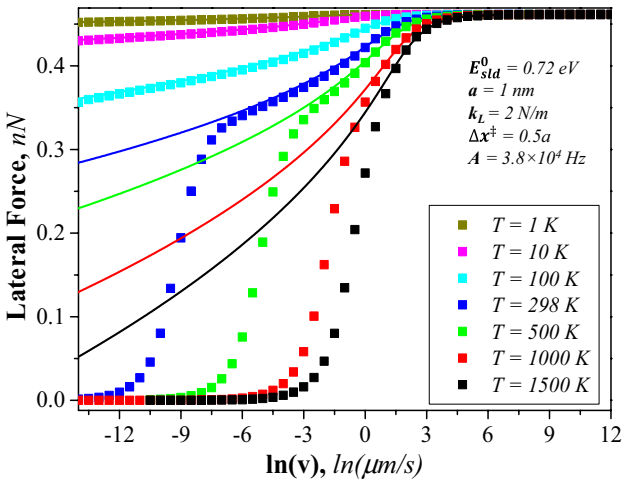

Fig. 5 Comparison between the analytical (Eq. (14), solid lines) and MC results (symbols), where backward and forward transitions are allowed, for the lateral force versus ln(v), at different temperatures

it does not consider where the tip will land after a previous transition. For example, if the tip arrives at a position that is higher than the detachment position predicted by the analytical model, the lateral force resulting from the subsequent transition will be higher than expected (see Supplementary Materials for more details). Finally, note that the curves tend to converge to a minimum value of lateral force as the velocity decreases (Fig. 4a). This can be explained by considering that, according to our model (when only considering forward transitions), the lowest possible lateral force that can be measured on a certain adsorption site is when the transition occurs as soon as a minimum to the right becomes available,

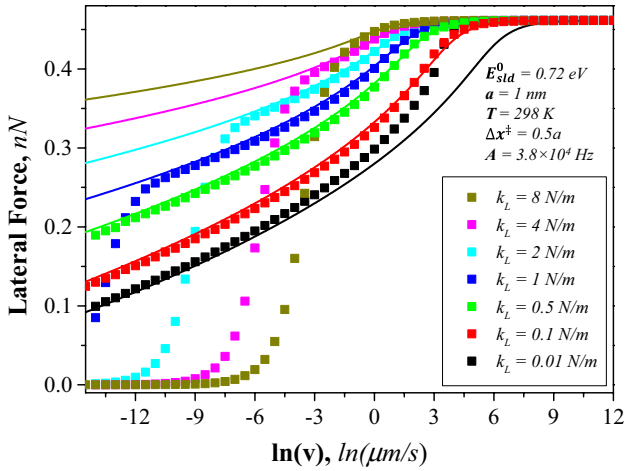

Fig. 6 Lateral force versus ln(v) for different values of k_L (or α for k_{sld} = 0.923 N/m). Equation (14) (solid lines) and MC results (symbols)

which in this case results in a minimum lateral force of ~ 0.17 nN (see Supplementary Materials for more details).

Since the Monte Carlo results have been proven to be consistent with the analytical model when only forward jumps are considered, this approach is used to study the effects of other phenomena such as backward transitions and the influence of the parameters E^0_{sld}, k_L and $\Delta x^{\ddagger}$. For comparison, the analytical results will be included along with the MC simulations.

Shown in Fig. 5 are the results of the MC simulations when allowing backward transitions to take place, where the parameters are the same as those used for Fig. 4. It can be observed that the MC simulations are in very good agreement with the analytic model at relatively high velocities and low temperatures, but show a rapid decrease in lateral force (with respect to the analytical results) as the velocity decreases and the temperature increases. This behavior is due to backward transitions (reattachment processes) occurring more often as the temperature increases and the sliding velocity decreases, thus deviating from the analytical solution, which only considers forward transitions (see Supplementary Materials for more details). In general, as expected, the lateral force increases with sliding velocity, up to a critical lateral force F^*, as well as a lateral force that decreases with temperature. Note that the lateral force tends to zero as the sliding velocity decreases, which is also expected given that the system is allowed to completely relax as sliding takes place.

Shown in Fig. 6 are the results obtained using the same parameters as in Fig. 5, but now varying the elastic force constant, k_L (E^0_{sld} = 0.72 eV, T = 298 K, a = 1 nm and $\Delta x^{\ddagger}$ = 0.5a). As can be observed, the value of k_L has a significant effect on the behavior of the lateral force. Although the general behavior remains the same as for the analytical model, a rapid drop in friction occurs at higher velocities as the value of k_L increases. This is due to that backward transitions are more likely, at a given velocity, as the value of k_L increases, allowing the system to become more relaxed as sliding takes place. Note that, at very small k_L values (e.g. 0.01 N/m), the simulated results are higher than those predicted by the analytical model, due to memory effects.

Figure 7 shows the MC results of lateral force versus ln (v) when varying the parameter $\Delta x^{\ddagger}$. The remaining parameters were kept constant (E^0_{sld} = 0.72 eV, T = 298 K, a = 1 nm and k_L = 2 N/m). Once again, there is always a good agreement with the analytical results, except for the friction drop due to the occurrence of backward transitions. Note that an increase in the critical force, F^*, is observed as the value of $\Delta x^{\ddagger}$ decreases. This can be easily explained given that a decrease in $\Delta x^{\ddagger}$ for the same value of E^0_{sld}, leads to a steeper parabolic

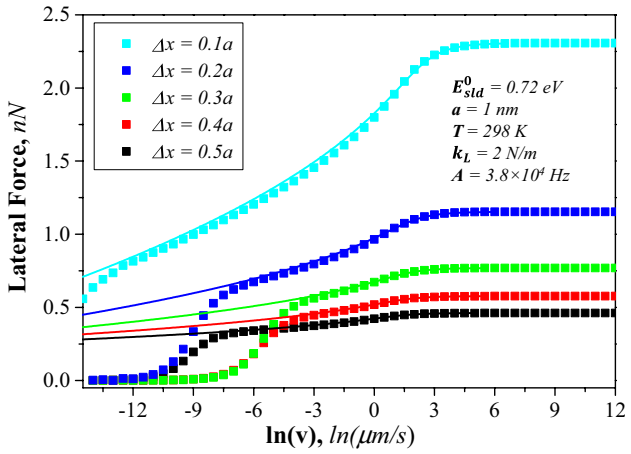

Fig. 7 Lateral force versus ln(v) for different values of $\Delta x^{\ddagger}$. Equation (14) (solid lines) and MC results (symbols)

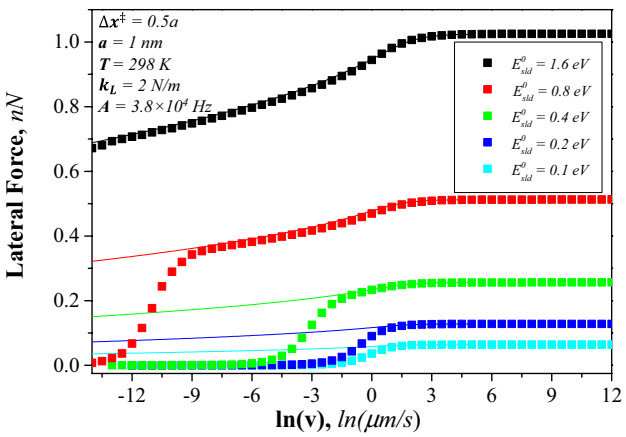

Fig. 8 Lateral force versus ln(v) for different values of E_0. Equation (14) (solid lines) and MC results (symbols)

potential, thus requiring more energy (force) for the tip to become detached from an adsorbate species and move in the sliding direction.

Finally, shown in Fig. 8 are the MC results of lateral force versus ln (v) when varying the parameter E^0_{sld} ($T=298$ K, $a=1$ nm, $k_{\mathrm{L}}=2$ N/m and $\Delta x^{\ddagger}=0.5a$). As expected, the critical force shows a linear increase with E^0_{sld}. Note that the drop in friction with respect to the analytical results occurs at lower velocities as the value of E^0_{sld} increases; this is again because backward transitions are less likely to occur as the sliding potential becomes steeper.

In order to establish an appropriate pre-exponential factor for the kMC simulations, the dynamics of the AFM tip can be taken into account by using the Langevin equation, which takes into account the dynamics over the energy barrier as well as the energy dissipation as the tip transits the barrier. The dynamics are governed by the equation [54, 61]:

$$m\ddot{x}+\gamma m\dot{x}=-\frac{\partial V_{\mathrm{tot}}}{\partial x}+\xi(t) \tag{17}$$

where m is the mass of the tip, γ is the viscous friction (or damping) coefficient per unit mass, and $\zeta(t)$ is a Gaussian random force and from Eq. (4), $V_{\mathrm{tot}}(x,t)=V_{\mathrm{S}}(x)+{}^1\!/_2 k_{\mathrm{L}}\left(v_X t-x\right)^2$.where $X=v_X t$ where v_X is the scan velocity and t is the time. It is usual to select the system to be critically damped to detect the stick–slip motion commonly found in AFM experiments [54, 62]. Under these conditions, the critical damping coefficient $\gamma_{\mathrm{C}}=2\sqrt{\frac{k_{\mathrm{sld}}+k_{\mathrm{L}}}{m}}=2\sqrt{\frac{k_{\mathrm{sld}}(1+\alpha)}{m}}$. Taking $m=1.8\times10^{-11}$ kg, yields a value of $\gamma_{\mathrm{C}}=5.33\times10^5\ \mathrm{s}^{-1}$. Kramers rate theory can be used to calculate the corresponding reaction pre-exponential factor $A=\kappa f_0$, where f_0 is an attempt frequency and κ is the transmission coefficient [61]. In the case of a smooth reaction profile, and writing the form of the potential for the initial state as $V_i(x)={}^1\!/_2\omega_i^2\left(x-x_i\right)^2$, where $\omega_i^2=\ddot{V}\left(x_i\right)/m$, and for the transition state is $V_t(x)=E_a-{}^1\!/_2\omega_t^2\left(x-x_t\right)^2$ and $\omega_t^2=\ddot{V}\left(x_t\right)/m$, $f_0=\frac{\omega_i}{2\pi}$ and $\kappa=\frac{1}{\omega_t}\left[\left(\frac{\gamma^2}{4}+\omega_t^t\right)^{1/2}-\frac{\gamma}{2}\right]$. The transmission coefficient for transition state with a cusp in the weak damping limit can be obtained by allowing $\omega_t\rightarrow\infty$ to give $\kappa=1$ while strong damping gives $\kappa=\frac{\omega_i}{\gamma}\left(\frac{\pi E_{\mathrm{a}}}{k_{\mathrm{B}}T}\right)^{1/2}$ [61]. The variation in transmission coefficient as a function of damping has been given by Pollak [63] as $\kappa=(1+B)^{1/2}-B^{1/2}$, where $B=\frac{k_{\mathrm{B}}T}{4\pi E_{\mathrm{a}}}\left(\frac{\gamma}{\omega_i}\right)^2$. In the case of a critically damped system, $\left(\frac{\gamma}{\omega_i}\right)=2$ so that $B_{\mathrm{crit}}=\frac{k_{\mathrm{B}}T}{\pi E_{\mathrm{a}}}$, and thus depends weakly on temperature and gives a value of $\kappa\sim0.9$ for an activation barrier of 0.72 eV for temperatures between 100 and 350 K, giving a pre-exponential factor $A\sim\frac{0.9}{2\pi}\sqrt{\frac{k_{\mathrm{sld}}+k_{\mathrm{L}}}{m}}$ and yields $3.8\times10^4\ \mathrm{s}^{-1}$.

4 Conclusions

This paper investigates the solution to a Prandtl–Tomlinson type friction model using parabolic sliding potential to mimic a sliding organic interface in which a compliant nanoscale contact attaches to and detaches from molecular adsorbate species. Such a potential is expected to be suitable for studying the frictional behavior of organic overlayers on surfaces and tribochemical reaction rates, and its simplicity allows it to be extended to coupled organic multilayer systems as well as being able to investigate the rate of shear-induced mechanochemical reactions. It may also be suitable for describing the dynamics of biological systems such as muscle motion and cellular transport proteins such as kinesin. This paper focusses on testing the validity of the analytical models by comparing the analytical results with kinetics Monte Carlo simulations. Applications to more realistic systems, such as the friction of adsorbed self-assembled monolayers will be deferred to subsequent publications.

A similar analytical model is derived for the velocity and temperature dependences of the friction force, which inherently only models motion in the sliding direction. The validity of the model is investigated using kinetic Monte Carlo methods for only forward sliding, where excellent agreement is found between the analytical model and the simulations, except for some slight differences that are identified and explained.

Kinetic Monte Carlo simulations that include both forward and reverse motion of the contact are also carried out, where good agreement is found with the analytical model for high sliding velocities and low temperatures, However, significant differences in the frictional behavior from the analytical model are found for other conditions, in particular where the friction force decreases to zero, providing superlubricious regimes that are not included in the analytical model. It is not clear how such effects might be easily incorporated into the analytical model and systems in which such effects are expected to be significant will have to be analyzed using kinetic Monte Carlo methods.

Supplementary Information The online version contains supplementary material available at https://doi.org/10.1007/s11249-021-01523-w.

Acknowledgements We gratefully acknowledge the Civil, Mechanical and Manufacturing Innovation (CMMI) Division of the National Science Foundation under Grant Nos. 1634340 and 2020525 for support of this work. GDK thanks the Fulbright Foundation for support of this work.

Author Contributions All authors contributed equally to this work.

Data Availability Data available in article or supplementary material.

Declarations

Ethical Approval All ethical responsibilities were respected by the authors.

References

1. Furlong, O.J., Miller, B.P., Kotvis, P., Tysoe, W.T.: Low-temperature, shear-induced tribofilm formation from dimethyl disulfide on copper. ACS Appl. Mater. Interfaces. **3**, 795–800 (2011)
2. Furlong, O., Miller, B., Tysoe, W.T.: Shear-induced boundary film formation from dialkyl sulfides on copper. Wear **274–275**, 183–187 (2012)
3. Miller, B., Furlong, O., Tysoe, W.: The kinetics of shear-induced boundary film formation from dimethyl disulfide on copper. Tribol. Lett. **49**, 39–46 (2013)
4. Adams, H.L., Garvey, M.T., Ramasamy, U.S., Ye, Z., Martini, A., Tysoe, W.T.: Shear-induced mechanochemistry: pushing molecules around. J. Phys. Chem. C **119**, 7115–7123 (2015)
5. Adams, H., Miller, B.P., Kotvis, P.V., Furlong, O.J., Martini, A., Tysoe, W.T.: In situ measurements of boundary film formation pathways and kinetics: dimethyl and diethyl disulfide on copper. Tribol. Lett. **62**, 1–9 (2016)
6. Adams, H., Miller, B.P., Furlong, O.J., Fantauzzi, M., Navarra, G., Rossi, A., et al.: Modeling mechanochemical reaction mechanisms. ACS Appl. Mater. Interfaces. **9**, 26531–26538 (2017)
7. Yeon, J., He, X., Martini, A., Kim, S.H.: Mechanochemistry at solid surfaces: polymerization of adsorbed molecules by mechanical shear at tribological interfaces. ACS Appl. Mater. Interfaces. **9**, 3142–3148 (2017)
8. Chen, L., Wen, J., Zhang, P., Yu, B., Chen, C., Ma, T., et al.: Nanomanufacturing of silicon surface with a single atomic layer precision via mechanochemical reactions. Nat. Commun. **9**, 1542 (2018)
9. Gosvami, N.N., Bares, J.A., Mangolini, F., Konicek, A.R., Yablon, D.G., Carpick, R.W.: Mechanisms of antiwear tribofilm growth revealed in situ by single-asperity sliding contacts. Science **348**, 102–106 (2015)
10. Felts, J.R., Oyer, A.J., Hernández, S.C., Whitener, K.E., Jr., Robinson, J.T., Walton, S.G., et al.: Direct mechanochemical cleavage of functional groups from graphene. Nat. Commun. **6**, 1–7 (2015)
11. Raghuraman, S., Elinski, M.B., Batteas, J.D., Felts, J.R.: Driving surface chemistry at the nanometer scale using localized heat and stress. Nano Lett. **17**, 2111–2117 (2017)
12. He, X., Kim, S.H.: Surface chemistry dependence of mechanochemical reaction of adsorbed molecules—an experimental study on tribopolymerization of α-Pinene on metal, metal oxide, and carbon surfaces. Langmuir **34**, 2432–2440 (2018)
13. Bell, G.: Models for the specific adhesion of cells to cells. Science **200**, 618–627 (1978)
14. Kuwahara, T., Romero, P.A., Makowski, S., Weihnacht, V., Moras, G., Moseler, M.: Mechano-chemical decomposition of organic friction modifiers with multiple reactive centres induces superlubricity of ta-C. Nat. Commun. **10**, 151 (2019)
15. Carpick, R.W., Salmeron, M.: Scratching the surface: fundamental investigations of tribology with atomic force microscopy. Chem. Rev. **97**, 1163–1194 (1997)
16. Gnecco, E., Bennewitz, R., Gyalog, T., Loppacher, C., Bammerlin, M., Meyer, E., et al.: Velocity dependence of atomic friction. Phys. Rev. Lett. **84**, 1172–1175 (2000)
17. Gnecco, E., Bennewitz, R., Gyalog, T., Meyer, E.: Friction experiments on the nanometre scale. J. Phys. **13**, R619–R642 (2001)
18. Bennewitz, R., Gnecco, E., Gyalog, T., Meyer, E.: Atomic friction studies on well-defined surfaces. Tribol. Lett. **10**, 51–56 (2001)
19. Tomlinson, G.A.: A molecular theory of friction. Philos. Mag. **7**, 905 (1929)
20. Prandtl, L.: Ein Gedankenmodell zur kinetischen Theorie der festen Körper. Z. Angew. Math. Mech. **8**, 85 (1928)
21. Sang, Y., Dube, M., Grant, M.: Thermal effects on atomic friction. Phys. Rev. Lett. **87**, 174301 (2001)
22. Riedo, E., Gnecco, E., Bennewitz, R., Meyer, E., Brune, H.: Interaction potential and hopping dynamics governing sliding friction. Phys. Rev. Lett. **91**, 084502 (2003)
23. Fusco, C., Fasolino, A.: Velocity dependence of atomic-scale friction: a comparative study of the one- and two-dimensional Tomlinson model. Phys. Rev. B **71**, 045413 (2005)
24. Socoliuc, A., Bennewitz, R., Gnecco, E., Meyer, E.: Transition from stick-slip to continuous sliding in atomic friction: entering a new regime of ultralow friction. Phys. Rev. Lett. **92**, 134301 (2004)
25. Porto, M., Zaloj, V., Urbakh, M., Klafter, J.: Macroscopic versus microscopic description of friction: from Tomlinson model to shearons. Tribol. Lett. **9**, 45–54 (2000)
26. Srinivasan, M., Walcott, S.: Binding site models of friction due to the formation and rupture of bonds: State-function formalism, force-velocity relations, response to slip velocity transients, and slip stability. Phys. Rev. E **80**, 046124 (2009)
27. Lacker, H.M., Peskin, C.S.: A mathematical method for the unique determination of cross-bridge properties from steady-state mechanical and energetic experiments on macroscopic muscle. Lectures Math. Life Sci. **16**, 32 (1986)
28. Huxley, A.F.: Muscle structure and theories of contraction. Prog. Biophys. Biophys. Chem. **7**, 255–318 (1957)
29. Filippov, A.E., Klafter, J., Urbakh, M.: Friction through dynamical formation and rupture of molecular bonds. Phys. Rev. Lett. **92**, 135503 (2004)
30. Barel, I., Urbakh, M., Jansen, L., Schirmeisen, A.: Temperature dependence of friction at the nanoscale: when the unexpected turns normal. Tribol. Lett. **39**, 311–319 (2010)
31. Barel, I., Urbakh, M., Jansen, L., Schirmeisen, A.: Unexpected temperature and velocity dependencies of atomic-scale stick-slip friction. Phys. Rev. B **84**, 115417 (2011)
32. Barel, I., Urbakh, M., Jansen, L., Schirmeisen, A.: Multibond dynamics of nanoscale friction: the role of temperature. Phys. Rev. Lett. **104**, 066104 (2010)
33. Eyring, H.: Viscosity, plasticity, and diffusion as examples of absolute reaction rates. J. Chem. Phys. **4**, 283–291 (1936)
34. Kauzmann, W., Eyring, H.: The viscous flow of large molecules. J. Am. Chem. Soc. **62**, 3113–3125 (1940)
35. Spikes, H., Tysoe, W.: On the commonality between theoretical models for fluid and solid friction wear and tribochemistry. Tribol. Lett. **59**, 1–14 (2015)
36. Bliznyuk, V.N., Everson, M.P., Tsukruk, V.V.: Nanotribological properties of organic boundary lubricants: langmuir films versus self-assembled monolayers. J. Tribol. **120**, 489–495 (1998)
37. Zhang, L., Leng, Y., Jiang, S.: Tip-based hybrid simulation study of frictional properties of self-assembled monolayers: effects of chain length, terminal group, scan direction, and scan velocity. Langmuir **19**, 9742–9747 (2003)
38. Tsukruk, V.V., Everson, M.P., Lander, L.M., Brittain, W.J.: Nanotribological properties of composite molecular films: C60 anchored to a self-assembled monolayer. Langmuir **12**, 3905–3911 (1996)
39. van der Vegte, E.W., Subbotin, A., Hadziioannou, G., Ashton, P.R., Preece, J.A.: Nanotribological properties of unsymmetrical

n-Dialkyl sulfide monolayers on gold: effect of chain length on adhesion, friction, and imaging. Langmuir **16**, 3249–3256 (2000)
40. Liu, Y., Evans, D.F., Song, Q., Grainger, D.W.: Structure and frictional properties of self-assembled surfactant monolayers. Langmuir **12**, 1235–1244 (1996)
41. Brewer, N.J., Beake, B.D., Leggett, G.J.: Friction force microscopy of self-assembled monolayers: influence of adsorbate alkyl chain length, terminal group chemistry, and scan velocity. Langmuir **17**, 1970–1974 (2001)
42. Pan, Y.-S., Xiong, D.-S., Ma, R.-Y.: A study on the friction properties of poly(vinyl alcohol) hydrogel as articular cartilage against titanium alloy. Wear **262**, 1021–1025 (2007)
43. Pan, Y., Xiong, D.: Friction properties of nano-hydroxyapatite reinforced poly(vinyl alcohol) gel composites as an articular cartilage. Wear **266**, 699–703 (2009)
44. Gong, J., Iwasaki, Y., Osada, Y., Kurihara, K., Hamai, Y.: Friction of Gels. 3. Friction on solid surfaces. J. Phys. Chem. B **103**, 6001–6006 (1999)
45. Chang, D.P., Dolbow, J.E., Zauscher, S.: Switchable friction of stimulus-responsive hydrogels. Langmuir **23**, 250–257 (2007)
46. Reale, E.R., Dunn, A.C.: Poroelasticity-driven lubrication in hydrogel interfaces. Soft Matter **13**, 428–435 (2017)
47. Shoaib, T., Espinosa-Marzal, R.M.: Insight into the viscous and adhesive contributions to hydrogel friction. Tribol. Lett. **66**, 96 (2018)
48. Weymouth, A.J., Hofmann, T., Giessibl, F.J.: Quantifying molecular stiffness and interaction with lateral force microscopy. Science **343**, 1120–1122 (2014)
49. Cappella, B., Dietler, G.: Force-distance curves by atomic force microscopy. Surf. Sci. Rep. **34**, 1–104 (1999)
50. Evans, M.G., Polanyi, M.: Some applications of the transition state method to the calculation of reaction velocities, especially in solution. Trans. Faraday Soc. **31**, 875–894 (1935)
51. Marcus, R.A.: On the theory of oxidation-reduction reactions involving electron transfer I. J. Chem. Phys. **24**, 966–978 (1956)
52. Gnecco, E., Bennewitz, R., Socoliuc, A., Meyer, E.: Friction and wear on the atomic scale. Wear **254**, 859–862 (2003)
53. Gnecco, E., Roth, R., Baratoff, A.: Analytical expressions for the kinetic friction in the Prandtl-Tomlinson model. Phys. Rev. B **86**, 035443 (2012)
54. Krylov, S.Y., Frenken, J.W.M.: The physics of atomic-scale friction: Basic considerations and open questions. Phys. Status Solidi B **251**, 711–736 (2014)
55. Furlong, O.J., Manzi, S.J., Pereyra, V.D., Bustos, V., Tysoe, W.T.: Kinetic Monte Carlo theory of sliding friction. Phys. Rev. B **80**, 153408 (2009)
56. Furlong, O.J., Manzi, S.J., Pereyra, V.D., Bustos, V., Tysoe, W.T.: Monte Carlo simulations for Tomlinson sliding models for non-sinusoidal periodic potentials. Tribol. Lett. **39**, 177–180 (2010)
57. Manzi, S., Tysoe, W., Furlong, O.: Temperature dependences in the Tomlinson/Prandtl model for atomic sliding friction. Tribol. Lett. **55**, 363–369 (2014)
58. Furlong, O., Manzi, S., Martini, A., Tysoe, W.: Influence of potential shape on constant-force atomic-scale sliding friction models. Tribol. Lett. **60**, 1–9 (2015)
59. Sales, J.L., Uñac, R.O., Gargiulo, M.V., Bustos, V., Zgrablich, G.: Monte Carlo simulation of temperature programmed desorption spectra: a guide through the forest for monomolecular adsorption on a square lattice. Langmuir **12**, 95–100 (1996)
60. Bondi, A.: Van der Waals volumes and dadii. J. Phys. Chem. **68**, 441–451 (1964)
61. Hänggi, P., Talkner, P., Borkovec, M.: Reaction-rate theory: fifty years after Kramers. Rev. Mod. Phys. **62**, 251–341 (1990)
62. Roth, R., Glatzel, T., Steiner, P., Gnecco, E., Baratoff, A., Meyer, E.: Multiple slips in atomic-scale friction: an indicator for the lateral contact damping. Tribol. Lett. **39**, 63–69 (2010)
63. Pollak, E.: Variational transition state theory for activated rate processes. J. Chem. Phys. **93**, 1116–1124 (1990)

Authors and Affiliations

Sergio Javier Manzi[1] · Sebastian Eduardo Carrera[1] · Octavio Javier Furlong[1] · Germaine Djuidje Kenmoe[2,3] · Wilfred T. Tysoe[3]

[1] Instituto de Física Aplicada (INFAP), CONICET-Universidad Nacional de San Luis, Chacabuco 917, 5700 San Luis, Argentina

[2] Department of Physics, Faculty of Science, University of Yaounde 1, P.O. Box 812, Yaounde, Cameroon

[3] Laboratory for Surface Studies, and Department of Chemistry and Biochemistry, University of Wisconsin-Milwaukee, Milwaukee, WI 53211, USA